

- Yellow highlights should be in math environment
- Green highlights indicate a missing space
- Blue highlights means a word should be hyphenated
- Red highlights are just to gain attention

Three cold gas filaments converging to a massive galaxy group at $z=2.91$: a case for gas infall

E. Daddi¹, F. Valentino², R.M. Rich³, D. Neill⁴, D. O'Sullivan⁴, M. Gronke⁵, D. Elbaz¹, F. Bournaud¹, A. Finoguenov⁶, S. Cantalupo⁷, A. Marchal⁸, I. Delvecchio¹, S. Jin⁹, D. Liu¹⁰, A. Calabro¹¹, R. Coogan¹², C. D'Eugenio¹, R. Gobat¹³, B.S. Kalita¹, P. Laursen¹⁴, D.C. Martin⁴, A. Puglisi¹⁵, E. Schinnerer¹⁰, V. Strazzullo¹⁶, T. Wang¹⁷

¹CEA, IRFU, DAp, AIM, Université Paris-Saclay, Université Paris Diderot, Sorbonne Paris Citè, CNRS, F-91191 Gif-sur-Yvette, France

²Cosmic Dawn Center (DAWN), Niels Bohr Institute, University of Copenhagen, Juliane Maries

Vej 30, DK 2100 Copenhagen DTU-Space, Technical University of Denmark, Elektrovej 327,

~~DK 2800 Kgs. Lyngby~~

³Department of Physics and Astronomy, University of California Los Angeles, 430 Portola Plaza, Los Angeles, CA 90095, USA

⁴California Institute of Technology, 1216 East California Boulevard, Pasadena, California 91125, USA.

⁵Department of Physics, University of California, Santa Barbara CA 93106, USA

⁶Department of Physics, University of Helsinki, Gustaf Hällstrmin katu 2, FI-00014 Helsinki, Finland

⁷Department of Physics, ETH Zurich, Wolfgang-Pauli-Strasse 27, CH-8093 Zurich, Switzerland

⁸Canadian Institute for Theoretical Astrophysics, University of Toronto, 60 St. George Street, Toronto, ON M5S 3H8, Canada.

⁹*Instituto de Astrofsica de Canarias (IAC), E-38205 La Laguna, Tenerife, Spain*

¹⁰*Max Planck Institute for Astronomy, Konigstuhl 17, D-69117 Heidelberg, Germany*

¹¹*INAF, Osservatorio Astronomico di Roma, via Frascati 33, 00078, Monteporzio Catone, Italy*

¹²*Max-Planck-Institut fr extraterrestrische Physik (MPE), Giessenbachstrasse 1, 85748 Garching, Germany*

¹³*Instituto de Fsica, Pontificia Universidad Catlica de Valparaso, Casilla, 4059, Valparaso, Chile
Institute of Theoretical Astrophysics, University of Oslo, PO Box 1029 Blindern, 0315 Oslo, Norway*

¹⁴*Institutt for Astrofysik, University of Oslo.*

¹⁵*Institute for Computational Cosmology, Durham University, South Road, Durham DH1 3LE, UK*

¹⁶*Faculty of Physics, Ludwig-Maximilians-Universitt, Scheinerstr. 1, 81679, Munich, Germany*

¹⁷*Institute of Astronomy, Graduate School of Science, The University of Tokyo, 2-21-1 Osawa, Mitaka, Tokyo 181-0015, Japan*

Cosmic gas penetration inside massive dark matter (DM) halos has been proposed as a fundamental process driving galaxy formation at high redshift^{1,2}, but convincing observational confirmations are lacking³. The latest generation, high resolution simulations now dispute whether streams can survive the interaction with the hot baryons in halos and remain stable^{4,5,6}. This uncertainty on the feeding of galaxy activity also limits our understanding of feedback processes^{7,8}. Ly α nebulae observed in the environs of virtually every distant QSO⁹ can hardly probe the physics of gas accretion, as in their hosting halos the QSO outflows should dominate¹⁰ over inflow rates by orders of magnitude¹¹. Here we report a 300 kpc-wide giant Ly α nebula centered on the massive galaxy group RO-1001 at z=2.91. Three cold gas filaments from the cosmic web, shining through Ly α , converge into the center of the po-

tential well of its $\sim 4 \times 10^{13} M_{\odot}$ DM halo, hosting $1200 M_{\odot} \text{ yr}^{-1}$ of star formation. The upper limits on AGN activity and overall energetics favour gravity as the primary Ly α powering source. The outwards accelerating filament kinematics and the prevalence of blue-shifted components in the Ly α spectra support a scenario of gas infall, with a first direct observation of the skeleton. The discovery of this nebula offers an opportunity to quantitatively test models of gas accretion and galaxy feeding^{4,5,6,12,13,14,15}.

Following the serendipitous discovery¹⁶ of a giant Ly α halo around the X-ray detected cluster Cl 1449 at $z=1.99$, we have used the Keck Cosmic Web Imager (KCWI) to search for redshifted Ly α in RO-1001, a massive group of galaxies at $z=2.91$. RO-1001 was selected in the COSMOS 2-square-degree field as a 12σ overdensity of optically faint radio sources, following a recently proposed technique¹⁷: it contains 3 VLA detections with $S_{3\text{GHz}} > 30\mu\text{Jy}$ and $z_{\text{phot}} > 2.5$ within a radius of $10''$ (80 kpc; proper scales are used throughout the paper), i.e. the size of a massive halo core^{18,19}. These three galaxies are also bright in ALMA submm imaging ($200\mu\text{m}$ rest-frame), i.e. they are highly star forming galaxies (not AGNs; cf. Methods). NOEMA CO[3-2] line observations confirm their $z_{\text{spec}} \sim 2.91$ (Methods; Table 1). We obtained 8.5h on source over a KCWI mosaic (covering $40'' \times 60''$, i.e. $300 \times 500 \text{ kpc}^2$), during observing campaigns in January 2018 and February 2019. The observations revealed faint low-surface brightness, large area Ly α filamentary structures that converge onto a bright Ly α nebula at the center of the potential well of the group (Figs.1, 2), with a total¹ $L_{\text{Ly}\alpha} = 1.8 \times 10^{44} \text{ erg s}^{-1}$, $\sim 6\times$ more luminous than the nebula in Cl 1449¹⁶. Three filaments can be readily recognised from the surface brightness profile of the

¹We correct the observed flux by a factor of 2, accounting¹⁴ for the cosmic opacity to $z = 2.9$

nebula (Figs.1, 2). The two most prominent, extending South-East and West of the nebula, respectively, appear to be traceable over a projected distance of 200 kpc from the core, at the current 3σ surface brightness limit of 10^{-19} erg s $^{-1}$ cm $^{-2}$ arcsec $^{-2}$, reconstructed from adaptive smoothing (Methods). A third structure that we can identify with a filament extends towards the North-West (Fig.1,2), likely affected by projection effects.

The halo mass of RO-1001 is estimated using three methods returning consistent results: (1) the integrated stellar mass of $5.4 \times 10^{11} M_{\odot}$ of its four most massive galaxies (Fig.2) above a mass completeness limit of $\log(M/M_{\odot}) > 10.8$ and scaled based on stellar to DM ratios (Methods) corresponds to $M_{\text{DM}} \sim 4-6 \times 10^{13} M_{\odot}$. (2) Herschel+ALMA reveal a total $L_{\text{IR}} = 1.2 \times 10^{13} L_{\odot}$ from star formation: scaling from the $z = 2.5$ cluster CL-1001¹⁹ this returns $M_{\text{DM}} \sim 4 \times 10^{13} M_{\odot}$ (accounting for the expected cosmic increase of the SFR over $z = 2.5-2.9$). (3) A blind (no free parameters) ^{four} X-ray measurement centered at the barycenter of the 4 massive galaxies returns a 3.1σ excess over the background corresponding to $M_{\text{DM}} \sim 4 \times 10^{13} M_{\odot}$ (contamination by X-rays from star formation is negligible, while no individual point-like X-ray source is present). RO-1001 thus appears comparably massive to Cl-1001 at $z = 2.51$, the previously most distant X-ray structure known.

RO-1001 falls close to the z - M_{DM} regime where cosmological cold flows might penetrate the hot halo, as inferred from simulations and models^{2,20} (while this should not happen at lower redshifts). This would not be surprising, given the ongoing $\text{SFR}=1200 M_{\odot} \text{ yr}^{-1}$ of the group galaxies (Methods). Theory predicts^{21,22} gas accretion from the IGM scaling as $M_{\text{DM}}^{1.15} \times (1+z)^{2.25-2.5}$, or about $10000 M_{\odot} \text{ yr}^{-1}$ in RO-1001. This would be largely sufficient to feed the ongoing SFR, provided

that a non-negligible fraction of the likely multi-phase inflows⁶ remains cold. Additionally, local cooling due to the interactions and shocks between the infalling gas and the hot cluster gas might also provide^{5,23} the required cold gas fuel for star formation. The Ly α emission does not appear to be generally centered on individual galaxies: the luminous core peaks in an empty region located at the center of the halo potential well (Fig. Ex. 5). The 150–200 kpc radius traced by filaments corresponds to a significant 50–70% (and up to 100% accounting for possible projection effects) fraction of the virial radius of its hosting DM halo ($R_v \sim 280$ kpc): their disappearance beyond the virial radius at our current sensitivities is consistent with modeling¹³. These filaments have substantial transverse diameters (50–70 kpc; 10"; ~ 20% of the virial radius), as expected for flows into the most massive halos, broadened due to their initially higher pressure and instabilities^{6,13}. The average surface brightness in the filaments is of order 1×10^{-18} erg s⁻¹ cm⁻² arcsec⁻², with a total area above this surface brightness limit of about 210 arcsec² (1.3×10^4 kpc²). Again, all of this is quite comparable to theory expectations¹³ given the hosting halo mass. The circularly averaged surface brightness profile follows $r^{-2.1}$ at large distances, consistent with predictions¹³.

As typically the case with giant Ly α nebulae, there are two crucial questions that arise concerning their nature: 1) what is the origin of the cold Ly α emitting gas? and 2) what is the energy source of the emission? In order to gather physical insights into these questions for the RO-1001 nebula, it is relevant to compare with nebulae found in QSO/radio-galaxy fields⁹, which can reach similar luminosities and maximum spatial extent. One crucial observable that is required to perform this comparison is an evaluation of the presence of AGNs/QSO in the RO-1001 field. In RO-1001 there is no evidence of ongoing (obscured or not) AGN activity from ultra-deep Chandra

and mid-IR constraints (Methods). A summary of relevant physical quantities and energetics comparing the RO-1001 nebula and QSO nebulae is reported in Table 2. Regarding question 1) on the origin of the gas, there are two main channels that need to be evaluated and, ideally, distinguished: cosmological inflows, mainly expected to be a function of the **DM halo mass** **and redshift**, and outflows from AGNs/galaxies, which depend on the AGN bolometric luminosity¹¹ and galaxy SFRs. For the case of the QSO nebulae, outflow rates are expected to exceed inflow rates by at least two orders of magnitude (Methods; Table 2), making the search for infalling gas in those systems very difficult. The situation is reversed for the case of RO-1001: given the AGN luminosity upper limits, infalling gas rates are expected to dominate outflow rates by almost one order of magnitude. Infalling gas could hence possibly be detected, while outflows could play some non-negligible role.

Regarding question 2) on the powering source, relevant channels are: ionization from AGN or star formation, dissipation of kinetic energy carried out by outflows from the same AGN/SFR, and gravitational energy. For the QSO nebulae, Ly α emission is generally assumed to be powered by fluorescence from QSO ionization, which indeed is the most energetic source. Based on Table 2 we argue that QSO outflows might also contribute a sizeable amount of energy: their role in QSO nebulae might have been underestimated so far. For RO-1001 the multi-wavelength limits to possible AGN activity, or even assuming ongoing AGN activity at the cosmic average given the stellar mass and SFR present, imply a net production rate of ionizing photons that is insufficient to account for the observed Ly α luminosity (Table 2; Methods). On the other hand, given the estimated DM halo mass, in RO-1001 we expect the available gravitational energy from infall to exceed all other source of energy by at least two orders of magnitudes (Table 2).

For clarity, I think this section would benefit from splitting the discussions of the various mechanisms in separate paragraphs.
I've indicated with a " \hookrightarrow " where I would suggest new lines.

The possibility that a bright QSO just switched off seems very unlikely: the probability of finding a luminous QSO associated with our massive galaxies is $< 10^{-4}$ (Methods), and a QSO nebula with a similar skeleton of three converging filaments has never been seen. \hookrightarrow Ly α powering from star formation should also be considered. Using deep Subaru Suprime-CAM imaging in VRI bands places a 5σ lower limit of $EW > 500\text{\AA}$ (rest-frame) on the diffuse Ly α equivalent width. This is high enough to exclude diffuse in-situ star formation (e.g., Ly α originating in large numbers of low mass star forming galaxies). \hookrightarrow Ionization from star formation of the ALMA-detected galaxies can also be excluded, as it requires that 20% of all the ionizing photons reach the diffuse HI gas. Because of dust attenuation, normal disk-like massive galaxies at $z \sim 3$ are expected to have only 0.16% ionizing radiation escape fraction²⁴. This number might actually be ~~over~~ conservative, as the ALMA sizes of the three highly ~~SH~~ galaxies are unusually small. Their half light radii are at the level of 800 pc (Methods), implying that the expected dust columns are very large and the escape fraction of ionizing photons likely virtually null. \hookrightarrow Finally, widespread cooling from the X-ray gas in the halo has already been rejected in the C11449 nebula¹⁶ as disfavored by energetics by many magnitudes orders of ~~mags~~ (in addition, this effect is largely redshift independent and should not be prevalently remove hyphen seen at high-~~z~~). \hookrightarrow In conclusion, energetic arguments strongly favor cooling via radiation-dissipated gravitational energy as the most plausible channel for the (collisional or shock) excitation of Ly α emission in RO-1001 nebula. In a RO-1001-like halo, the emerging Ly α radiation powered by gravitational energy has been predicted by existing models¹⁴ to be of the order of 10^{44}erg s^{-1} , fully consistent with what is observed here, and at the level of few percent of the total available gravitational energy (Methods; Table 2).

We can search for confirming evidence of the ongoing physical processes from the Ly α spectral properties. The moment 1 (velocity) map of the Ly α emission in RO-1001 is shown in Fig.3a. The velocity relative to the core increases in absolute value towards the outer region of the filaments reaching 400-500 km s $^{-1}$ (and possibly up to 600-700 km s $^{-1}$ when statistically correcting for the unknown inclinations), similar to virial velocity and as predicted by theory^{6,13}. This is evidence for infall along the filaments where the initial (virial) velocity is progressively reduced as the flows proceed in the hot medium with which they interact: just like outflows decelerate when proceeding from their launching sites in galaxies into the hot circumgalactic medium²⁵. Any attempt to reproduce this feature with outflows would need to be excessively fine-tuned. Some existing inflow~~X~~ models¹⁵ fall short of predicting the velocity gradient that we observe along the filaments from the outskirts to the core. A possibility for reconciling to those predictions would be to assume projection effects where the gradient arise from the bending of the filaments inside the halo.

The moment-2 (velocity dispersion; Fig.3b) map shows a typical velocity dispersion at the level of 200-300 km s $^{-1}$, about half of the virial velocity (classifying RO-1001 as a *cold* nebula) but higher than the expected thermal broadening of the cold $\sim 10^4$ K gas (few tens km s $^{-1}$), as expected⁶ for multiphased, cloudy accretion flows in which streams do not remain highly collimated. It is also characterised by a distinctive pattern in which the dispersion is decreasing towards the outskirts likely due to decreasing turbulence towards the virial radius.

The observed velocity gradient between the edge of the filaments and the core together with

the velocity dispersion increasing towards the core allows us to obtain a rough estimate of the cold gas mass flow, assuming that the initial kinetic energy of the cold gas ($\dot{M}v_{\text{virial}}^2$) is partly transformed into turbulence ($\dot{M}\sigma_{\text{turbulence}}^2$) and partly radiated away (mainly via Ly α). Our numbers suggest that 10-30% of the initial energy is converted into turbulence⁶, with a cold mass flow rate of 1000-2000 M_{\odot} yr⁻¹, thus a penetration efficiency²¹ of 10-20%. This infall rate approximates the ongoing SFR, but only a fraction of this will effectively reach the galaxies, consistent with the requirement that the system must be heading to a downfall of the activity in a few dynamical timescales (few Gyr), and eventually quench.

The typical spectra of the Ly α emission in the core of the nebula is reported in Fig.4b, showing a double peaked shape, with the blue component stronger than the red one. This is reversed from what observed in most Ly α emitting galaxies²⁶ where the observation of a stronger red peak is associated to outflows²⁷, hence here suggesting infall. We modeled the spectra accounting for radiative transfer effects using the *tlac* code (Methods), assuming the (admittedly simplistic) geometry of a shell. For both spectra the fitting suggests moderately low column densities of neutral hydrogen HI, at the level of a few 10^{17} atoms cm⁻², suggesting fairly reduced radiative transfer effects implying that the inferred systemic velocities and dispersions previously measured from the blueshift-dominated Ly α moments are reliable, as often observed in Ly α blobs²⁸. The blue-shifted dominated spectral shape requires an overall average infalling velocity of $v_{\text{infall}} \sim 150$ km s⁻¹. The systemic velocity is close to our zero-velocity scale, which is defined as the Ly α flux weighted velocity of the full nebula, and is consistent with the average CO[3-2] redshifts of the 3 ALMA galaxies. This implies that such emission originates from gas at rest with respect to the center of the potential well, on

average. It would be very important to confirm this feature with observations of non-resonant lines.

Several hotter regions with $400\text{-}500 \text{ km/s}$ dispersion are evident (red spots in Fig. 3b): it is tempting to interpret them as possible shock fronts from the incoming material surrounding the core regions where gas density is highest. Modeling with *tlac* supports this idea, recovering higher HI column densities at one of the most conspicuous locations (Fig.4d).

For a region around the galaxy 'A' the spectral shape is reversed (Fig.4c), with the red component being stronger. This red-dominated spectrum is fitted as originating at a systemic velocity of 326 km s^{-1} ; shifted in the direction of the CO[3-2] velocity inferred for the underlying galaxy 'A' (460 km s^{-1}). It is difficult to distinguish such velocity offset as due to relative motion with respect to the center of the system, or due to a Hubble flow effect that would require a physical separation of about 1 Mpc on the line of sight. The prevalence of the red peak suggests in any case, an overall outflowing velocity of $v_{\text{outflow}} \sim 200 \text{ km s}^{-1}$. The red-core emission is thus best understood as coming from outflows likely originating from galaxy 'A'. It is plausible that infall and outflows co-exist nearly everywhere. Estimated global motions with their signs likely reflect the local balance between the two processes. Still, if the spectrum in Fig.4c originates from galaxy 'A' the modest velocity offsets and flow-velocities suggest star-formation driven outflows (consistent with our estimates in Table 2), given that for AGN driven ones some $1000\text{-}2000 \text{ km s}^{-1}$ velocity offsets would be expected.

It would be very instructive to be able to carry out a detailed spectral analysis also along the filaments, evaluating whether their spectral shape is also mostly blue-shifted. However, they

are detected at high SNRs only in the lower resolution data. We thus decompose pixel-by-pixel with double Gaussians the lower resolution Ly α spectra over the whole nebula, using ROHSA (Methods), a code that allows for regularization and stability of the solution, in the assumption of slowly varying parameters across the field. We obtain spatially resolved maps of the ratio of red-shifted to blue-shifted components (Fig.4a), that can be used to gauge where infall vs. outflows might prevail. The result of this analysis is that infall appears to dominate also along the filaments, except a few regions that appear to be instead dominated by outflows, similarly to the core.

In the light of these results it is relevant to re-evaluate which process might be responsible for the Ly α emission. The classic expectation would be collisionally excited Ly α from the cold gas dissipating the gravitational energy. In order to be viable this would require a fairly high neutral fraction in the gas³. The HI column density inferred from Ly α modeling is not very high but appears to be sufficient for the purpose: even assuming that Ly α is photoionized by some unknown source, the inferred ionized hydrogen column density would be of the same order of magnitude²⁹, assuming the cold gas is in pressure equilibrium with the cluster hot phase. Hence in all cases the neutral fraction seem to be sufficiently high in this halo. We notice though that an alternative possibility is that radiation is emitted through Kelvin Helmholtz (or RayleighTaylor) instabilities at the interface between the streaming gas and the hot halo gas^{5,6} ensuing local cooling and production of additional cold gas. In that case Ly α radiation would originate from the combined dissipation of kinetic energy of the stream and of thermal energy from the hot gas that cools down.

In summary, RO-1001 at $z = 2.91$ is currently the most distant bona-fide X-ray group known

and, to our knowledge, also the first plausible case of direct observations of gas accretion towards a massive potential well (Fig.Ex.3). It is not surprising that, finally, a reasonable case for infall has been found in a massive high-redshift group, which is where gas accretion should be strongest, and the contrast of inflows over outflows the highest. Filaments have been claimed to exist³⁰ also in the well known SSA22a-LAB1 protocluster environment but the relative nebula is not consistent with arising from infall²⁸ and the filaments are situated at locations that are impossible to directly connect to DM halos. Knowledge of mass and position of the center of mass of the RO-1001 group is a crucial information that was not available for other known filamentary nebulae and sets a clear new precedent for future research along this line.

References

1. Kereš, D., Katz, N., Weinberg, D. H., Davé, R. 2005. How do galaxies get their gas?. Monthly Notices of the Royal Astronomical Society 363, 2-28.
2. Dekel, A., Birnboim, Y., Engel, G., Freundlich, J., Goerdt, T., Mumcuoglu, M., Neistein, E., Pichon, C., Teyssier, R., Zinger, E. 2009. Cold streams in early massive hot haloes as the main mode of galaxy formation. Nature 457, 451-454.
3. Cantalupo, S. 2017. Gas Accretion and Giant Ly α Nebulae. Gas Accretion onto Galaxies 430, 195.
4. Nelson, D., Genel, S., Vogelsberger, M., Springel, V., Sijacki, D., Torrey, P., Hernquist, L. 2015. The impact of feedback on cosmological gas accretion. Monthly Notices of the Royal

- Astronomical Society 448, 59-74.
5. Mandelker, N., Nagai, D., Aung, H., Dekel, A., Padnos, D., Birnboim, Y. 2019. Instability of supersonic cold streams feeding Galaxies - III. Kelvin-Helmholtz instability in three dimensions. Monthly Notices of the Royal Astronomical Society 484, 1100-1132.
 6. Cornuault, N., Lehnert, M. D., Boulanger, F., Guillard, P. 2018. Are cosmological gas accretion streams multiphase and turbulent?. Astronomy and Astrophysics 610, A75.
 7. Gabor, J. M., Bournaud, F. 2014. Delayed star formation in high-redshift stream-fed galaxies. Monthly Notices of the Royal Astronomical Society 437, L56-L60.
 8. Dekel, A., Mandelker, N. 2014. An analytic solution for the minimal bathtub toy model: challenges in the star formation history of high-z galaxies. Monthly Notices of the Royal Astronomical Society 444, 2071-2084.
 9. Borisova, E., and 19 colleagues 2016. Ubiquitous Giant Ly α Nebulae around the Brightest Quasars at z~3.5 Revealed with MUSE. The Astrophysical Journal 831, 39.
 10. Guo, Y., and 10 colleagues 2020. Metal enrichment in the circumgalactic medium and Ly α haloes around quasars at z ~3. arXiv e-prints arXiv:2001.05473.
 11. Fiore, F., and 16 colleagues 2017. AGN wind scaling relations and the co-evolution of black holes and galaxies. Astronomy and Astrophysics 601, A143.

12. Goerdt, T., Dekel, A., Sternberg, A., Ceverino, D., Teyssier, R., Primack, J. R. 2010. Gravity-driven Ly α blobs from cold streams into galaxies. *Monthly Notices of the Royal Astronomical Society* 407, 613-631.
13. Rosdahl, J., Blaizot, J. 2012. Extended Ly α emission from cold accretion streams. *Monthly Notices of the Royal Astronomical Society* 423, 344-366.
14. Dijkstra, M., Loeb, A. 2009. Ly α blobs as an observational signature of cold accretion streams into galaxies. *Monthly Notices of the Royal Astronomical Society* 400, 1109-1120.
15. Danovich, M., Dekel, A., Hahn, O., Ceverino, D., Primack, J. 2015. Four phases of angular-momentum buildup in high-z galaxies: from cosmic-web streams through an extended ring to disc and bulge. *Monthly Notices of the Royal Astronomical Society* 449, 2087-2111.
16. Valentino, F., and 19 colleagues 2016. A Giant Ly α Nebula in the Core of an X-Ray Cluster at $Z = 1.99$: Implications for Early Energy Injection. *The Astrophysical Journal* 829, 53.
17. Daddi, E., and 17 colleagues 2017. Radio Selection of the Most Distant Galaxy Clusters. *The Astrophysical Journal* 846, L31.
18. Strazzullo, V., and 10 colleagues 2013. Galaxy Evolution in Overdense Environments at High Redshift: Passive Early-type Galaxies in a Cluster at $z \sim 2$. *The Astrophysical Journal* 772, 118.
19. Wang, T., and 19 colleagues 2016. Discovery of a Galaxy Cluster with a Violently Starbursting Core at $z = 2.506$. *The Astrophysical Journal* 828, 56.

20. Behroozi, P., Silk, J. 2018. The most massive galaxies and black holes allowed by Λ CDM. Monthly Notices of the Royal Astronomical Society 477, 5382-5387.
21. Dekel, A., Zolotov, A., Tweed, D., Cacciato, M., Ceverino, D., Primack, J. R. 2013. Toy models for galaxy formation versus simulations. Monthly Notices of the Royal Astronomical Society 435, 999.
22. Neistein, E., Dekel, A. 2008. Merger rates of dark matter haloes. Monthly Notices of the Royal Astronomical Society 388, 1792-1802.
23. Zinger, E., Dekel, A., Birnboim, Y., Nagai, D., Lau, E., Kravtsov, A. V. 2018. Cold fronts and shocks formed by gas streams in galaxy clusters. Monthly Notices of the Royal Astronomical Society 476, 56.
24. Pannella, M., and 27 colleagues 2015. GOODS-Herschel: Star Formation, Dust Attenuation, and the FIR-radio Correlation on the Main Sequence of Star-forming Galaxies up to $z \approx 4$. The Astrophysical Journal 807, 141.
25. Steidel, C. C., and 7 colleagues 2010. The Structure and Kinematics of the Circumgalactic Medium from Far-ultraviolet Spectra of $z \approx 2-3$ Galaxies. The Astrophysical Journal 717, 289.
26. Orlitová, I., and 6 colleagues 2018. Puzzling Lyman-alpha line profiles in green pea galaxies. Astronomy and Astrophysics 616, A60.
27. Kulas, K. R., Shapley, A. E., Kollmeier, J. A., Zheng, Z., Steidel, C. C., Hainline, K. N. 2012. The Kinematics of Multiple-peaked Ly α Emission in Star-forming Galaxies at $z \sim 2-3$. The Astrophysical Journal 745, 33.

28. Herenz, E. C., Hayes, M., Scarlata, C. 2020. Deciphering Lyman α blob 1 with deep MUSE observations. arXiv e-prints arXiv:2001.03699.
29. Hennawi, J. F., Prochaska, J. X. 2013. Quasars Probing Quasars. IV. Joint Constraints on the Circumgalactic Medium from Absorption and Emission. *The Astrophysical Journal* 766, 58.
30. Umehata, H., and 17 colleagues 2019. Gas filaments of the cosmic web located around active galaxies in a protocluster. *Science* 366, 97.

Methods

KCWI observations and analysis. We observed RO-1001 with KCWI on January 16th 2018 for 1h using the BM grism ($R = 2000$ with the adopted large field of view), and on February 3rd and 4th 2019 for 3.5h and 4h respectively using the lower resolution BL grism ($R = 900$), giving a total 8.5h on source when combining all observations. Conditions were excellent with dark sky and seeing typically in the range of 0.4–0.7''. We used integration times of 900s in 2018 and of 1800s in 2019, with dithering and large offsets to eventually cover a region corresponding to \sqrt{times} 2×2 KCWI fields of view. In fact, already with the first 1h integration obtained in 2018 it was clear that the nebula extends well beyond the usable KCWI field of view of about $18 \times 31''$ for the adopted configuration with large slices (1.35''). The low resolution BL data covers the full 3500–5500Å range (corresponding to 900–1400Å rest-frame at the redshift of RO-1001), while the BM observations cover a shorter range across the Ly α emission. We used the standard KCWI pipeline *Kderp*^{31,32} for the data reduction, including twilight flats to obtain accurate illumination corrections. We further use *CubEx* tools³³ to refine the flat-fielding slice by slice, thus allowing us to improve the sky subtraction by removing a median sky value at each wavelength layer, after masking sources detected in the stacked (continuum) cubes. This step was first performed over the whole frame and subsequently iterated by masking regions where Ly α emission had been detected, to avoid self-subtraction of the Ly α signal. Further reduction and analysis steps were performed with the *CWItools* scripts³⁴. We estimate variance cubes from the original, $none$ no-resampled cubes and propagate the uncertainties through the combination to obtain a final variance cube. We combined the dithered and offset observations based on the astrometry of each frame that was derived by

cross-correlating to B-band Suprime CAM imaging of the area publicly available from the COS-MOS survey, and resampling into a final pixel scale of $0.29''$, corresponding to the finer grid in the original slices. We then subtracted any continuum emission from objects in the combined cubes by fitting a 7th order polynomial as a function of wavelength at each spatial pixel, avoiding the wavelength range where $\text{Ly}\alpha$ emission is present. From compact objects in the final cube we estimate an average image quality of $0.6''$ (FWHM). The $\text{Ly}\alpha$ nebula is very clearly detected. We produced a low-resolution cube containing all 8.5h observations, used for most of the analysis in this paper, and a higher spectral resolution cube using only 2018 BM data, used to obtain higher quality $\text{Ly}\alpha$ spectra in the core (Fig.4). We used adaptive smoothing^{34,35} to recover the full extent of the nebula in the low resolution cube, thresholding at the 3σ level. We started by smoothing with a spatial kernel equal to the seeing and averaging three (1\AA wide) spectral layers (roughly corresponding to the spectral resolution). This already selects 93% of the pixels eventually detected in the $\text{Ly}\alpha$ nebula when allowing for larger spatial and spectral smoothing scales. We use the adaptively smoothed cube for subsequent analysis in this paper.

$\text{Ly}\alpha$ radiative transfer modeling. We compared the measured $\text{Ly}\alpha$ spectra to synthetic ones which were generated using the ‘shell-model’. The ‘shell-model’ consists of a moving concentric shell of neutral hydrogen and dust which surrounds a central $\text{Ly}\alpha$ (and continuum) emitting source. This setup introduces at least five parameters: the neutral hydrogen column density N_{HI} , the dust optical depth τ_d , the velocity of the shell v_{exp} (defined to be positive when outflowing), the (effective) temperature of the shell T (incorporating any small-scale turbulence), and the width of the intrinsic Gaussian line σ_i .

Specifically, we fitted the observed (continuum-subtracted) Ly α spectrum using the improved *tlac* pipeline³⁶. This pipeline consists of 12,960 models covering the (N_{HI} , v_{exp} , T) parameter space, and the other parameters are modeled in post-processing. To the five parameters above, we also added the systemic redshift which we allowed to vary within $[-700, 400]$ km s $^{-1}$ (corresponding to the velocity range spanned by individual CO[3-2] detections in the group) of $z = 2.9154$ (the average, flux weighted, Ly α velocity). Furthermore, we modeled the effect of the spectral resolution by smoothing the synthetic spectra with a Gaussian with FWHM of 150 km s $^{-1}$.

In order to sample the posterior distribution sufficiently, we used the tempered affine invariant Monte Carlo sampler of the Python package `emcee`³⁷. We chose to employ 10 temperatures, 200 walkers, and 2000 steps which we found to be sufficient to sample the posterior.

Ly α double Gaussian decomposition. We model the Ly α emission of the nebula $I(\nu)$ in the low-resolution cube using ROHSA³⁸. ROHSA is a multi-Gaussian decomposition algorithm based on a regularized nonlinear least-square criterion that takes into account the spatial coherence of the emission. Here we choose to decompose the signal into a sum of $N=2$ Gaussians, in order to capture the basic effects of resonant scattering, producing blue-shifted and red-shifted components (Fig.4). The model of the emission is then

$$\tilde{I}(\nu, \theta(r)) = \sum_{n=1}^{N=2} G(\nu, \theta_n(r)), \quad (1)$$

with $\theta(r) = (\theta_1(r), \dots, \theta_n(r))$ and where

$$G(\nu, \theta_n(r)) = a_n(r) \exp\left(-\frac{(\nu - \mu_n(r))^2}{2\sigma_n(r)^2}\right) \quad (2)$$

is parametrized by $\theta_n = (a_n, \mu_n, \sigma_n)$ with $a_n \geq 0$ being the amplitude, μ_n the position, and σ_n the standard deviation 2D maps of the n -th Gaussian profile. The estimated parameters $\hat{\theta}$ are obtained by minimizing the cost function as described in Reference 38. The latter includes a Laplacian filtering to penalize the small-scale fluctuation of each 2D map of parameters. Note that in order to perform this minimization, the whole emission cube is fitted at once. The strength of this filtering is controlled by three hyper-parameters $\lambda_a=10$, $\lambda_\mu=4000$, and $\lambda_\sigma=4000$. These parameters have been empirically chosen to obtain a spatially coherent solution of $\hat{\theta}$ with the smallest residual $\tilde{I}(\nu, \theta(r)) - I(\nu)$. We obtained a median absolute residual of 2.3%, showing that $N=2$ provides a good spatially coherent description of the signal.

Stellar masses and hosting halo mass. There are four massive ($M > 10^{11} M_\odot$) galaxies within 13'' (~100 kpc proper at $z = 2.91$) of RO-1001, with an estimated^{39,40} photometric redshift in the range $2.5 < z < 3.5$, see Table 1. One source (D in Fig.2) is blended with a close neighbour. We obtained a revised stellar mass estimate, empirically calibrated on sources at similar redshift from the COSMOS2015 catalog³⁹, and based on J, H, K photometry from the DR4 UltraVISTA imaging and 3.6, 4.5 μm Spitzer/IRAC imaging. We estimate a stellar mass completeness limit of $\log(M/M_\odot)=10.8$ (we assume a Chabrier IMF throughout this paper).

Three of the massive galaxies are shown to be at $z = 2.91$ from CO[3-2] spectroscopy, but source D remains unidentified as it is likely passive. Given the similarity in the colors and SED to other group members we will assume in the following of the paper that it also resides in the RO-1001 group.

There are no further $z \sim 3$ massive galaxies out to a distance of 1' from RO-1001. The total stellar mass of $\log(M/M_\odot) > 10.8$ galaxies in the structure thus adds up to $5.4_{-0.5}^{+2} \times 10^{11} M_\odot$, where we assumed that the uncertainty on individual stellar mass estimates is at least a factor $\sim 50\%$, see e.g. Reference 40. We extrapolate a total stellar mass down to $10^7 M_\odot$ of $1.0_{-0.2}^{+0.7} \times 10^{12} M_\odot$ assuming the stellar mass function (muzzin2013) of field galaxies at $2.5 < z < 3$. Adopting the scaling between total stellar and halo mass derived⁴¹ from $z \sim 1$ clusters with masses in the range $0.6 - 16 \times 10^{14} M_\odot$, would yield a halo mass of $M_{200} \sim 6 \times 10^{13} M_\odot$. We note that if scaling by the difference between the cluster and field galaxy stellar mass function at $z \sim 1$ as in reference 42, we would obtain a lower total stellar mass of $7.6_{-1.5}^{+5} \times 10^{11} M_\odot$, and thus a lower total halo mass of $M_{200} \sim 4 \times 10^{13} M_\odot$. However, the environmental dependence of stellar mass functions at $z \sim 1$ and $z \sim 3$ may be significantly different, so a range of $M_{200} \sim 4 - 6 \times 10^{13} M_\odot$ brackets the range of plausible estimates. We note that the stellar mass to DM mass scaling that we obtain is fully similar to what is estimated for Cl-1001 and for Cl-1449, which are supported by X-ray detections^{43,19} and SZ for Cl 1449⁴⁴.

In order to search for X-ray emission from the hot gas at the position of RO-1001, we used an X-ray image in the 0.5-2 keV range, produced by combining the Chandra and XMM-Newton images after background and point source removal. We used a 24'' radius aperture to place the flux estimates on the source, obtaining a value of 5.8×10^{-16} ergs s⁻¹ cm⁻², which is at 3.1σ excess over the background. The source has a 230ks Chandra exposure, with a corresponding upper limit on the point source contamination of 1×10^{-16} ergs s⁻¹ cm⁻² (using the same count-rate to flux-conversion-rate as for the source). At a redshift of $z = 2.9$ this corresponds⁴⁵ to rest-frame 0.1-2.4

subscript

keV L_X of 1.1×10^{44} erg s⁻¹ and a mass of $M_{\text{DM}} \sim 4 \times 10^{13} M_{\odot}$. The estimated temperature of the ICM is 2.1 keV.

Star formation activity. The total IR luminosity of the group is derived by fitting⁴⁶ Herschel, SCUBA2, and ALMA and NOEMA continuum fluxes. The Herschel/SPIRE images are fitted using two PSF components on the images on the position of sources C and the average position of A and B, respectively. Due to the higher spatial resolution, we fit at the position of all 3 ALMA sources in the SCUBA2 image (Fig. Ex.4, 5). We fit the SED of the group, including the summed photometry from Spitzer, Herschel, SCUBA2, ALMA and NOEMA, and obtain a best fitting SFR = $1200 M_{\odot} \text{ yr}^{-1}$ for a SED with an average intensity of the radiation field $\langle U \rangle = 45$ (Fig. Ex 4). Both the dust temperature and average specific star formation rate (sSFR; 3 Gyr⁻¹ on average over the 3 ALMA galaxies) are in agreement with those of typical Main Sequence galaxies at $z \sim 3$ (Bethermin et al 2015). Assuming that individual SFRs of the ALMA-detected galaxies scale like the ALMA/NOEMA continuum fluxes, we conclude that also the sSFRs of the individual galaxies place them within the Main Sequence.

The ALMA 870 μm emission from the 3 detected galaxies is consistent within the uncertainties to the SCUBA2 signal (Fig. Ex 4), implying that the bulk of the IR emission and SFR in the cluster comes from the 3 ALMA detections.

We identified additional star forming galaxies in the structure at $z = 2.91$ via their Ly α emission, or in two cases via possible UV absorption lines (Fig. Ex. 6). They are not detected in the near-IR to current depths, implying they are lower-mass, star-forming galaxies.

ALMA and NOEMA observations. We recovered all available ALMA band 7 data covering RO-1001, which consist of three pointings from projects 2015.1.00137.S (PI: N. Scoville) and 2016.1.00478.S (PI: O. Miettinen). They are imaged with a common restoring beam of 0.15 arcsec with natural weighting (given the maximum baseline of 1107 m), then corrected for primary beam attenuation and combined. The continuum rms reaches about $50 \mu\text{Jy beam}^{-1}$ in the central region at the restored resolution (and about $\times 2$ higher if tapering to a beam of $0.6''$). Three galaxies are very strongly detected (Fig.Ex.1; Table1). No other significant detection is present in the ALMA imaging.

In order to measure the size of the dust emission, we modeled the ALMA observations in the UV space, combining all datasets, following a well established method(Puglisi). We fitted circular Gaussian sources for simplicity: sizes for individual objects are reported in Table 2.

We observed the RO-1001 field with the IRAM NOEMA interferometer covering the CO[3-2] line emission redshifted to 88.3 GHz for $z = 2.91$, with the main aims of confirming the redshift of cluster galaxies and measuring accurately their systemic velocities. The field was observed during November 2018 to March 2019. A total of 7 tracks were obtained. The data was calibrated in a standard way using GILDAS *clic* software packages, and analysed with *mapping*. The image has an rms sensitivity of $5 \mu\text{Jy}/\text{beam}$ in the continuum and of 24 mJy km s^{-1} over 300 km s^{-1} for emission lines. The primary beam is about 1 arcmin, thus covering a large area around the nebula. The resulting synthesized beam at 88.3 GHz is rather elongated with $4.0 \times 1.8''$, with a position angle of 15° . None of the ALMA detected sources is resolved at this resolution. We thus extracted their spectra by fitting PSFs in the UV space at the known spatial positions from ALMA.

We simultaneously fit all galaxies in the field, i.e. the three ALMA galaxies and a bright interloper falling by chance in the large NOEMA field, in order to avoid being affected by sidelobes. The continuum is strongly detected in all the **three** ALMA sources in the cluster. We searched for emission lines in the spectra by identifying channel ranges with excess positive emission and identified the strongest line in each galaxy spectrum as the one with the lowest chance significance^{47,48}. Sources B and C have very strong CO[3-2] detections with $SN \sim 14$ at $z = 2.91$ and very broad emission lines with full width zero intensity of FWZI $\sim 1000 \text{ km s}^{-1}$. For source A the strongest feature in its spectrum is a fairly weak, 3.5σ emission with 380 km s^{-1} of FWZI. While in itself its reality could be questionable, it turns out that this feature is offset by only 460 km s^{-1} from the average Ly α velocity from the cluster ($z = 2.91540$), when we cover CO[3-2] over about 50000 km s^{-1} in total. The probability of a line with such SNR to be found by chance so close to the structure redshift is **about 1%**. If we also take into account that the weak line falls almost exactly on top of the Ly α velocity at the position of the galaxy (See Fig.3a), we conclude that the identification of this weak feature as CO[3-2] is quite certain, and thus the redshift of the galaxy from the simultaneous detection of CO[3-2] and Ly α . A summary of the properties of the three detections by ALMA and NOEMA is given in Table 1.

We note that there are large variations in the CO[3-2] flux to underlying continuum ratio (Table 1). These can be due to several reasons, including variations in the dust temperature and/or CO excitation ratios. They might also be connected to rapid SFR variations given that the dust continuum characteristic timescale is 50-100 Myr while the CO[3-2] line is sensitive to the instantaneous dense gas content. However, we note that galaxy A has the lowest CO[3-2] to dust continuum

ratio, and is also the most compact: a factor of two smaller in radius than the other two (which are also extremely compact already). We speculate that the lack of CO[3-2] might be due to high optical depths as recently claimed for high-z dusty galaxies⁴⁸.

fourth-most

The 4th massive galaxy in the system (object D) remains undetected in ALMA and NOEMA continuum and has no CO[3-2] detection. Assuming the average SED temperature as seen in the group to convert the ALMA upper limits into SFR, we place an upper limit of $SFR < 30M_{\odot} \text{ yr}^{-1}$ ($\text{sSFR} < 0.3 \text{ Gyr}^{-1}$), that locates this galaxy one dex below the Main Sequence. It is thus a candidate quiescent system in the group.

AGN limits. A cross-match between RO 1001 and the deepest Chandra COSMOS+Legacy images⁴⁹ yields no X-ray point-source detection. We stacked the observed soft (0.5-2 keV) and hard (2-10 keV) bands at the position of the 3 ALMA sources using CSTACK². We estimate an average $L_X < 3.5 \times 10^{43} \text{ erg s}^{-1}$ (3 σ upper limit) in the rest-frame 2-10 keV directly from the soft X-ray fluxes (0.5-2keV observed). The observed hard X-ray emission maps directly into 8-40keV rest-frame and is much less affected by obscuration. It provides a limit of $L_X < 5.4 \times 10^{43} \text{ erg s}^{-1}$ in the rest-frame 2-10 keV, K-corrected assuming a power-law X-ray spectrum with photon index Γ (Reference 50). When spread over the 3 sources, this gives an integrated limit of $L_X < 1.5 \times 10^{44} \text{ erg s}^{-1}$ in the rest-frame 2-10 keV. We further estimated 3 σ L_X upper limits of $L_X < 7 \times 10^{42} \text{ erg s}^{-1}$ (rest-frame 0.5-2 keV) corresponding to an AGN bolometric luminosity of $L_{\text{AGN}} < 2 \times 10^{45} \text{ erg s}^{-1}$, fairly independent on obscuration. This is corroborated by analysis of the individual broad-band SEDs⁴⁵, in which the mid-IR AGN component is always negligible relative

²CSTACK is publicly available at: <http://lambic.astrosen.unam.mx/cstack/>

to the host galaxy, providing similar limits on any possible AGN bolometric luminosity.

We further calculated the average L_X expected from the integrated SFR of the group/cluster, assuming empirical M_\star -dependent L_X /SFR relations^{51–53} for star-forming galaxies, arriving again at a very similar number. On average, we would expect from this structure an AGN activity at the level of $L_{\text{AGN}} \sim 2 \times 10^{45} \text{ erg s}^{-1}$. We use this number for our energetics estimates.

Using modeling⁵² that reproduces the evolution of the X-ray luminosity function through cosmic time on the basis of the mass-function and SFR distributions statistically observed in galaxies, we infer that, given the massive galaxies in the RO-1001 structure and their SFRs, the probability to observe one of them with QSO luminosities as high as those in Borisova is of the order of 10^{-4} . This shows that the duty cycle during which our RO-1001 group could be selected as part of the QSO nebulae surveys is very reduced.

The RO-1001 structure was selected due to the presence of three VLA-detected sources at 3 GHz. All have moderate radio power $L_{\text{3GHz}} \sim 10^{24.2-24.6} \text{ W Hz}^{-1}$. Given the integrated SFR of the group/cluster ($\sim 1200 M_\odot \text{ yr}^{-1}$) and a redshift-dependent infrared-radio correlation(Delhaize), radio emission can be broadly explained by consistent levels of star formation within less than a factor of 2 (Fig. Ex. 4). Source C contains a weak radio feature elongated to the W, visible at 3 GHz, which might trace (past or relatively weak) AGN activity in this source. This is consistent with the weak Ly α (Fig.1, 2) and HST i-band continuum (Fig.Ex.6) detections of this galaxy.

Energetics. We consider that the energy released from Ly α in the RO-1001 nebula could come from AGN and/or SF photoionization, from AGN and/or SF outflows, or from the release of grav-

itational energy. All our calculations are summarized in Table 2.

For the case of photoionization, the observed Ly α luminosity corresponds to $\sim 1.5 \times 10^{55}$ ionizing photons. Scaling from Cl 1449 calculations¹⁶, this ionizing photon rate requires $L_{\text{AGN}} \sim 3.5 \times 10^{45} \text{ erg s}^{-1}$. In the RO-1001 nebula our limit on AGN activity implies that < 60% of the required photons are produced. When considering that the typical Lyman continuum escape for moderate AGNs is $\sim 30\%$, and that not all photons are likely usable due to geometry constraints, covering factors, missing period etc, we conclude that AGN ionization cannot produce the observed Ly α . The output from the on-going SFR from the 3 ALMA galaxies is potentially capable of producing 5 times more ionizing photons than required to ionize the nebulae. However, as argued in the main text, these galaxies are extremely obscured. Even assuming typical attenuation properties of normal galaxies of the same mass would imply that only 1.6×10^{-3} of the ionizing photons actually escape the galaxy. This number could be orders of magnitude smaller if these sources are obscured like typical SMGs^{46,54,55}, as IR-luminous massive galaxies at high-z tend to be^{56,57}. The same argument thus applies to resonant scattering of photons from any AGN/SF activity, which cannot dominate, given the lack of sources producing sufficient primary hard UV photons that can escape the galaxies ISM. We emphasize that, unlike AGNs, light attenuation in star forming galaxies is not expected to be anisotropic (it is not driven by a torus), as demonstrated, e.g., by the tight relation^{58,59} between dust extinction and stellar mass. The amount of UV rest-frame emission observed from galaxies in the RO-1001 structure corresponds to a totally negligible fraction of the required ionizing photons, even neglecting further differential attenuation with respect to the UV.

The outflow rate from possible AGNs in the structure can be estimated following scaling

mass

laws¹¹, while for star formation we can assume a loading factor of 1. We further assume typical velocities of 500 km s^{-1} (1000 km s^{-1}) for SF(AGN) outflows to infer that these outflows would carry out of the galaxies roughly as much energy as what observed in Ly α . However, only a small ...Ly α . Hence... fraction of this energy would emerge reprocessed by Ly α hence we expect that outflows could contribute something locally, but not dominate. Ly α , also cannot come from in-situ X-ray cooling even under local thermal runaway instabilities, as the Xray/Lya luminosity ratio is way too small, as already discussed for Cl 1449¹⁶.

Finally, we compute the total gravitational energy. For the dark matter halo estimated for RO-1000, the energy associated⁶⁰ with cosmological gas accretion is $160\times$ what is required to power the nebula.

It is interesting to perform similar calculations for typical QSO nebulae⁹, see Table 2. We conservatively assume average hosting halo masses of $3\times 10^{12} M_\odot$ that are at the upper limits of the plausible range (most likely⁶¹ value of $1\times 10^{12} M_\odot$). In this case the available gravitational energy is barely comparable to the energy required to power the nebulae, hence it plays quite clearly a negligible role given the overall poor efficiency of converting such energy into Ly α photons. On the other hand, QSOs produce 40 \times more photons than needed to power the relative nebulae, and outflows from the luminous QSO roughly a similar additional amount. Hence it is quite clear that such nebulae are powered by QSO photoionization as widely recognised³, although QSO outflows could also play an important role.

References

31. Morrissey, P., and 38 colleagues 2018. The Keck Cosmic Web Imager Integral Field Spectrograph. *The Astrophysical Journal* 864, 93.
32. Neill, J. D., Matuszewski, M. 2018, KCWI Data Reduction Pipeline: First Minor Release, Zenodo, doi:10.5281/zenodo.1287322
33. Cantalupo, S., and 13 colleagues 2019. The large- and small-scale properties of the intergalactic gas in the Slug Ly α nebula revealed by MUSE He II emission observations. *Monthly Notices of the Royal Astronomical Society* 483, 5188-5204.
34. O'Sullivan, D., Martin, C., Hamden, E., Matuszewski, M., Neill, D., Parihar, P., Lin, Z. 2019. FLASHES: Revealing the CGM around 50 z=2-3 QSOs. *American Astronomical Society Meeting Abstracts #233* 233, 128.06.
35. Martin, D. C., and 15 colleagues 2019. Multi-filament gas inflows fuelling young star-forming galaxies. *Nature Astronomy* 3, 822-831.
36. Gronke, M., Bull, P., Dijkstra, M. 2015. A Systematic Study of Lyman- α Transfer through Outflowing Shells: Model Parameter Estimation. *The Astrophysical Journal* 812, 123.
37. Goodman, J., Weare, J. 2010. Ensemble samplers with affine invariance. *Communications in Applied Mathematics and Computational Science* 5, 65.
38. Marchal, A., Miville-Deschénes, M.-A., Orieux, F., Gac, N., Soussen, C., Lesot, M.-J., d'Allonnes, A. R., Salomé, Q. 2019. ROHSA: Regularized Optimization for Hyper-Spectral

- Analysis. Application to phase separation of 21 cm data. *Astronomy and Astrophysics* 626, A101.
39. Laigle, C., and 36 colleagues 2016. The COSMOS2015 Catalog: Exploring the $1 \leq z \leq 6$ Universe with Half a Million Galaxies. *The Astrophysical Journal Supplement Series* 224, 24.
40. Muzzin, A., Marchesini, D., Stefanon, M., Franx, M., Milvang-Jensen, B., Dunlop, J. S., Fynbo, J. P. U., Brammer, G., Labb  , I., van Dokkum, P. 2013. A Public K_s -selected Catalog in the COSMOS/ULTRAVISTA Field: Photometry, Photometric Redshifts, and Stellar Population Parameters. *The Astrophysical Journal Supplement Series* 206, 8.
41. van der Burg, R. F. J., Muzzin, A., Hoekstra, H., Wilson, G., Lidman, C., Yee, H. K. C. 2014. A census of stellar mass in ten massive haloes at $z \sim 1$ from the GCLASS Survey. *Astronomy and Astrophysics* 561, A79.
42. van der Burg, R. F. J., and 11 colleagues 2013. The environmental dependence of the stellar mass function at $z \sim 1$. Comparing cluster and field between the GCLASS and UltraVISTA surveys. *Astronomy and Astrophysics* 557, A15.
43. Gobat, R., and 12 colleagues 2011. A mature cluster with X-ray emission at $z = 2.07$. *Astronomy and Astrophysics* 526, A133.
44. Gobat, R., and 11 colleagues 2019. Sunyaev-Zel'dovich detection of the galaxy cluster Cl J1449+0856 at $z = 1.99$: The pressure profile in uv space. *Astronomy and Astrophysics* 629, A104.

45. Leauthaud, A., and 29 colleagues 2010. A Weak Lensing Study of X-ray Groups in the Cosmos Survey: Form and Evolution of the Mass-Luminosity Relation. *The Astrophysical Journal* 709, 97-114.
46. Jin, S., and 19 colleagues 2018. Super-deblended Dust Emission in Galaxies. II. Far-IR to (Sub)millimeter Photometry and High-redshift Galaxy Candidates in the Full COSMOS Field. *The Astrophysical Journal* 864, 56.
47. Jin, S., Daddi, E., Magdis, G. E., Liu, D., Schinnerer, E., Papadopoulos, P. P., Gu, Q., Gao, Y., Calabro, A. 2019. Discovery of four cold dusty galaxies at $z=3.62-5.85$ in the COSMOS field: direct evidence of CMB impact on high-redshift galaxy observables. *arXiv e-prints* arXiv:1906.00040.
48. Coogan, R. T., and 15 colleagues 2018. Merger-driven star formation activity in Cl J1449+0856 at $z = 1.99$ as seen by ALMA and JVLA. *Monthly Notices of the Royal Astronomical Society* 479, 703-729.
49. Civano, F., and 41 colleagues 2016. The Chandra Cosmos Legacy Survey: Overview and Point Source Catalog. *The Astrophysical Journal* 819, 62.
50. Gilli, R., Comastri, A., Hasinger, G. 2007. The synthesis of the cosmic X-ray background in the Chandra and XMM-Newton era. *Astronomy and Astrophysics* 463, 79-96.
51. Delvecchio I, et al., 2019, submitted
52. Mullaney, J. R., Daddi, E., Béthermin, M., Elbaz, D., Juneau, S., Pannella, M., Sargent, M. T., Alexander, D. M., Hickox, R. C. 2012. The Hidden “AGN Main Sequence”: Evidence for a

- Universal Black Hole Accretion to Star Formation Rate Ratio since $z \sim 2$ Producing an M_{BH} - M_* Relation. *The Astrophysical Journal* 753, L30.
53. Rodighiero, G., and 14 colleagues 2015. Relationship between Star Formation Rate and Black Hole Accretion At $Z = 2$: the Different Contributions in Quiescent, Normal, and Starburst Galaxies. *The Astrophysical Journal* 800, L10.
54. Calabrò, A., and 20 colleagues 2019. Deciphering an evolutionary sequence of merger stages in infrared-luminous starburst galaxies at $z \sim 0.7$. *Astronomy and Astrophysics* 623, A64.
55. Calabrò, A., and 20 colleagues 2018. Near-infrared Emission Lines in Starburst Galaxies at $0.5 < z < 0.9$: Discovery of a Merger Sequence of Extreme Obscurations. *The Astrophysical Journal* 862, L22.
56. Elbaz, D., and 15 colleagues 2018. Starbursts in and out of the star-formation main sequence. *Astronomy and Astrophysics* 616, A110.
57. Puglisi, A., and 22 colleagues 2019. The Main Sequence at $z \sim 1.3$ Contains a Sizable Fraction of Galaxies with Compact Star Formation Sizes: A New Population of Early Post-starbursts?. *The Astrophysical Journal* 877, L23.
58. Garn, T., Best, P. N. 2010. Predicting dust extinction from the stellar mass of a galaxy. *Monthly Notices of the Royal Astronomical Society* 409, 421-432.
59. Kashino, D., and 28 colleagues 2013. The FMOS-COSMOS Survey of Star-forming Galaxies at $z \sim 1.6$. I. H α -based Star Formation Rates and Dust Extinction. *The Astrophysical Journal* 777, L8.

60. Faucher-Giguère, C.-A., Kereš, D., Dijkstra, M., Hernquist, L., Zaldarriaga, M. 2010. Ly α Cooling Emission from Galaxy Formation. *The Astrophysical Journal* 725, 633-657.
61. Pezzulli, G., Cantalupo, S. 2019. A high baryon fraction in massive haloes at $z \geq 3$. *Monthly Notices of the Royal Astronomical Society* 486, 1489.
62. Schulze, A., Silverman, J. D., Daddi, E., Rujopakarn, W., Liu, D., Schramm, M., Mainieri, V., Imanishi, M., Hirschmann, M., Jahnke, K. 2019. No signs of star formation being regulated in the most luminous quasars at $z \sim 2$ with ALMA. *Monthly Notices of the Royal Astronomical Society* 488, 1180-1198.

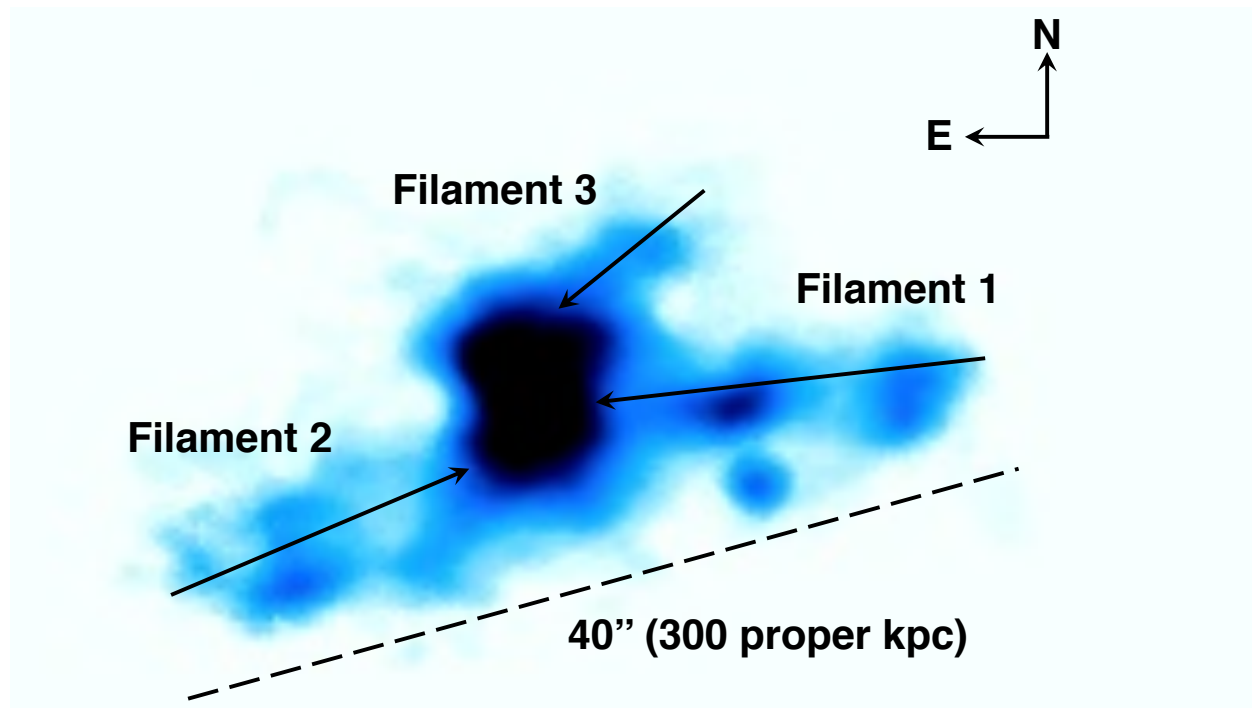


Figure 1: Ly α image from KCWI observations of the RO-1001 group. The three filaments clearly traced by Ly α are labeled. North is up and East is left. Corresponding Ly α surface brightness levels can be gauged from Fig.2.

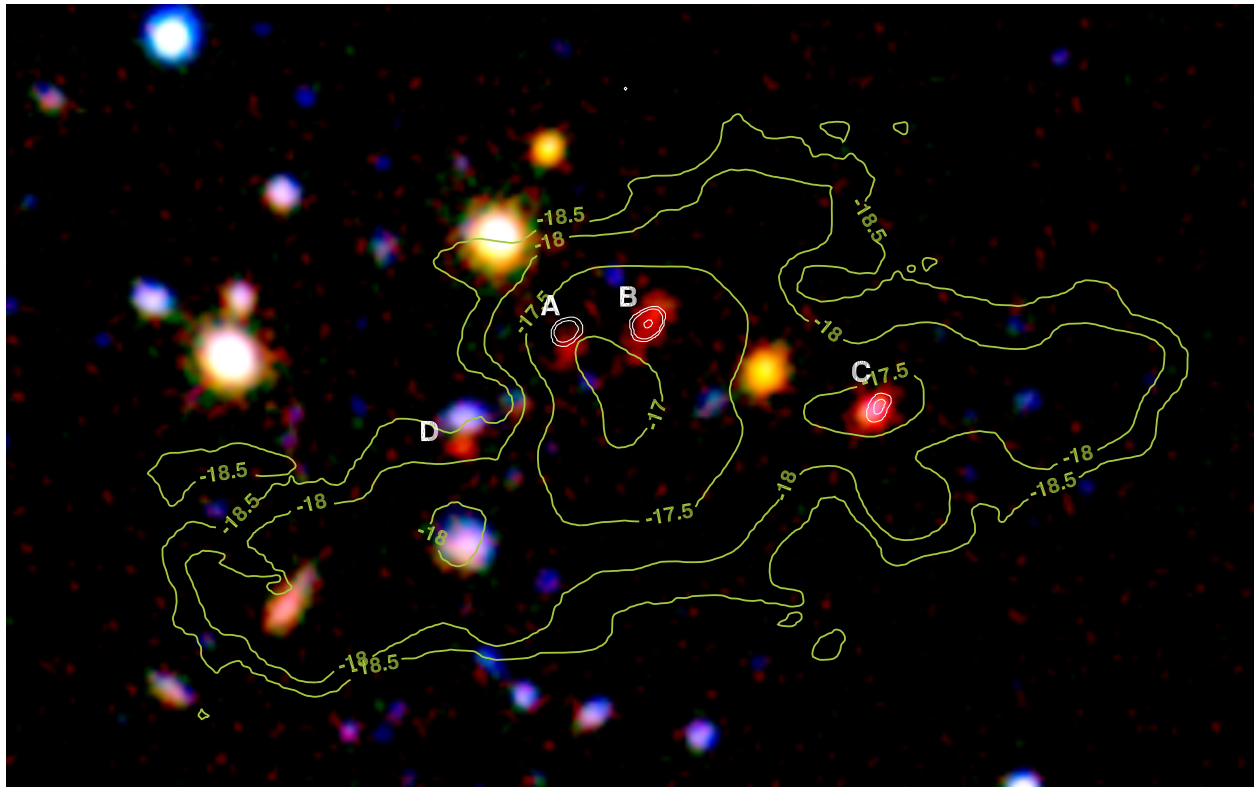


Figure 2: Deep optical-near-infrared imaging of the RO-1001 group from ULTRA-Vista K and J (red and green) and Subaru Suprime CAM (combined VRI bands; blue), over a $30'' \times 40''$ field of view. The contours show the Ly α surface brightness (SB) scale from Figure 2 in steps of 0.5 dex, from a few 10^{-17} erg cm $^{-2}$ s $^{-1}$ arcsec $^{-2}$ (center) to $\times 10$ lower SB (filaments). The 3 ALMA/VLA sources are labeled (ABC), together with a fourth massive galaxy (D) that is a candidate quiescent object in the structure.

UltraVISTA

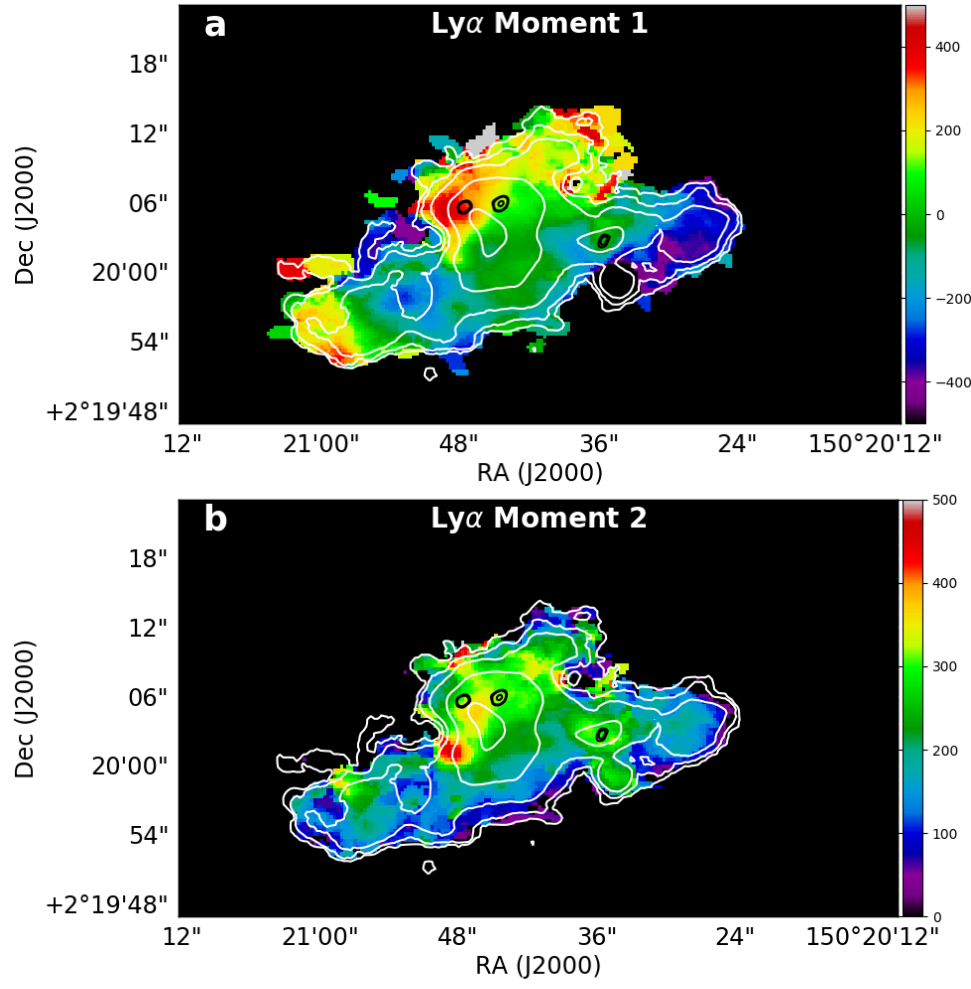


Figure 3: Ly α velocity map (top; moment 1) and velocity dispersion map (bottom; moment 2). Colorbar ~~X~~ levels of both maps (right scale) are expressed in km s $^{-1}$. ALMA sources contours are shown as black contours, in all panels. White contours show the Ly α SB levels from Fig.1. both

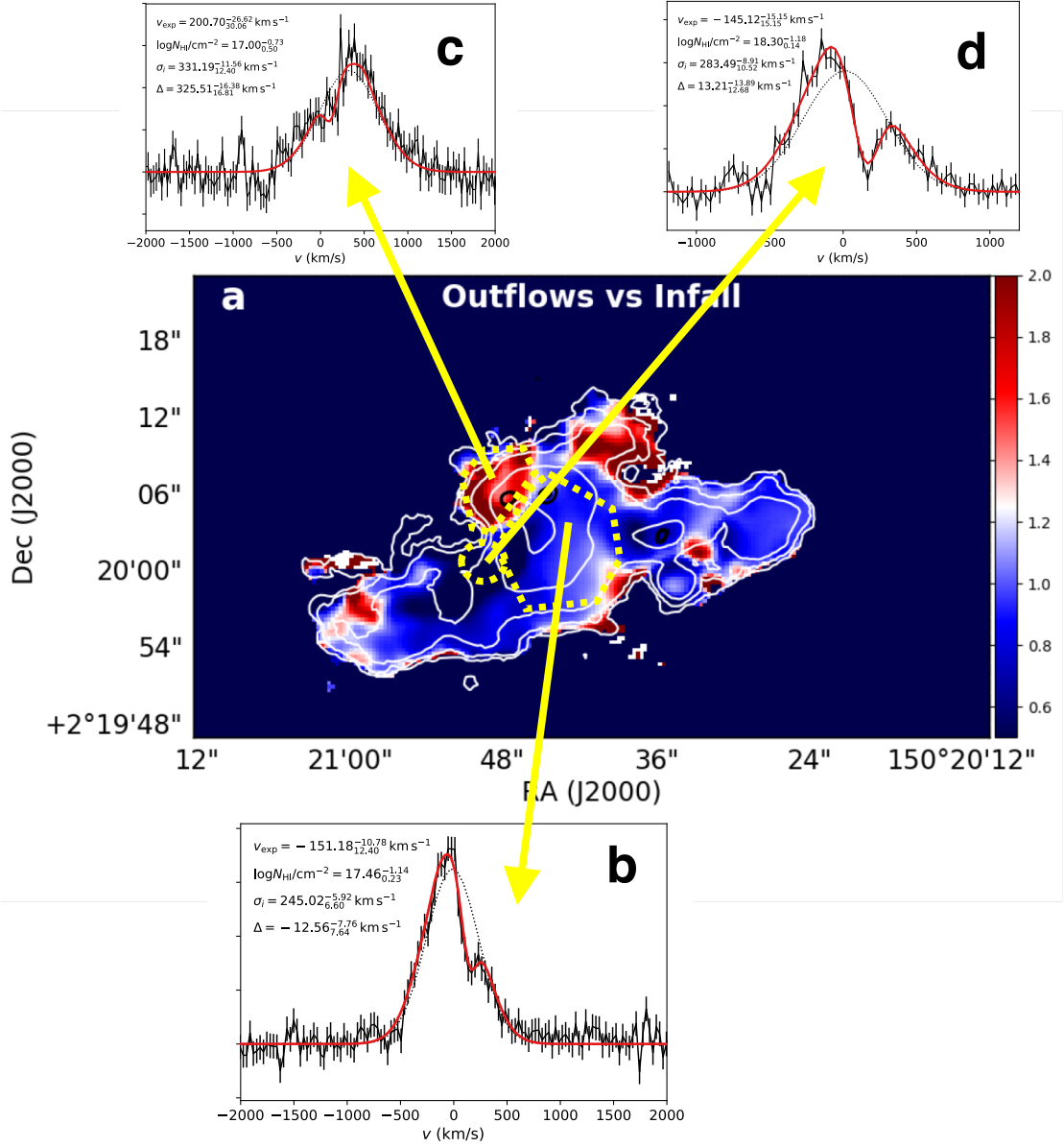


Figure 4: The color coding in the image (right scale) shows the ratio between red-shifted and blue-shifted components (Panel a) from a ROHSA analysis of the deeper low spectral resolution data. Blue (red) colors correspond to infall (outflow) dominated regions. ALMA sources contours are shown as black contours. White contours show the Ly α SB levels from Fig.1. Yellow-dotted contours show region where spectra were extracted, using the higher spectral resolution data, as shown in Panels b,c,d. Observed spectra are shown in black while best fitting *tlac* modeling is shown in red. Resulting constraints on physical quantities are labeled. Spectrum in Panel b shows a prominent blue peak and is integrated over most of the core of the nebula, with the exception of the NE corner whose spectrum is shown in Panel c and is characterised by a prominent red peak. Panel d shows the region with the largest velocity dispersion from Fig.3b.

The spectrum...

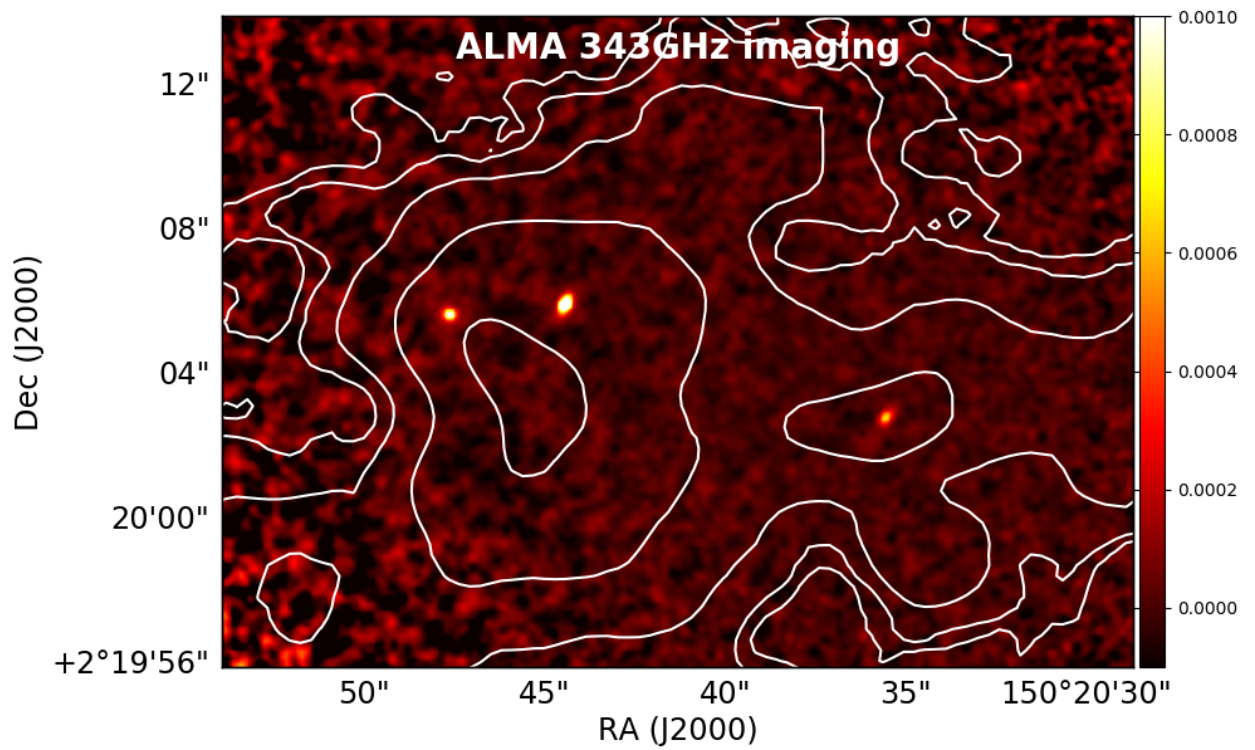


Figure Ex. 1: ALMA 343 GHz continuum mosaic image with primary beam attenuation correction (the colorbar shows Jy beam^{-1}). The image reaches an rms of $\sim 50 \mu\text{Jy beam}^{-1}$ at the center, at the resolution of $0.15''$. Contours show the Ly α emission.

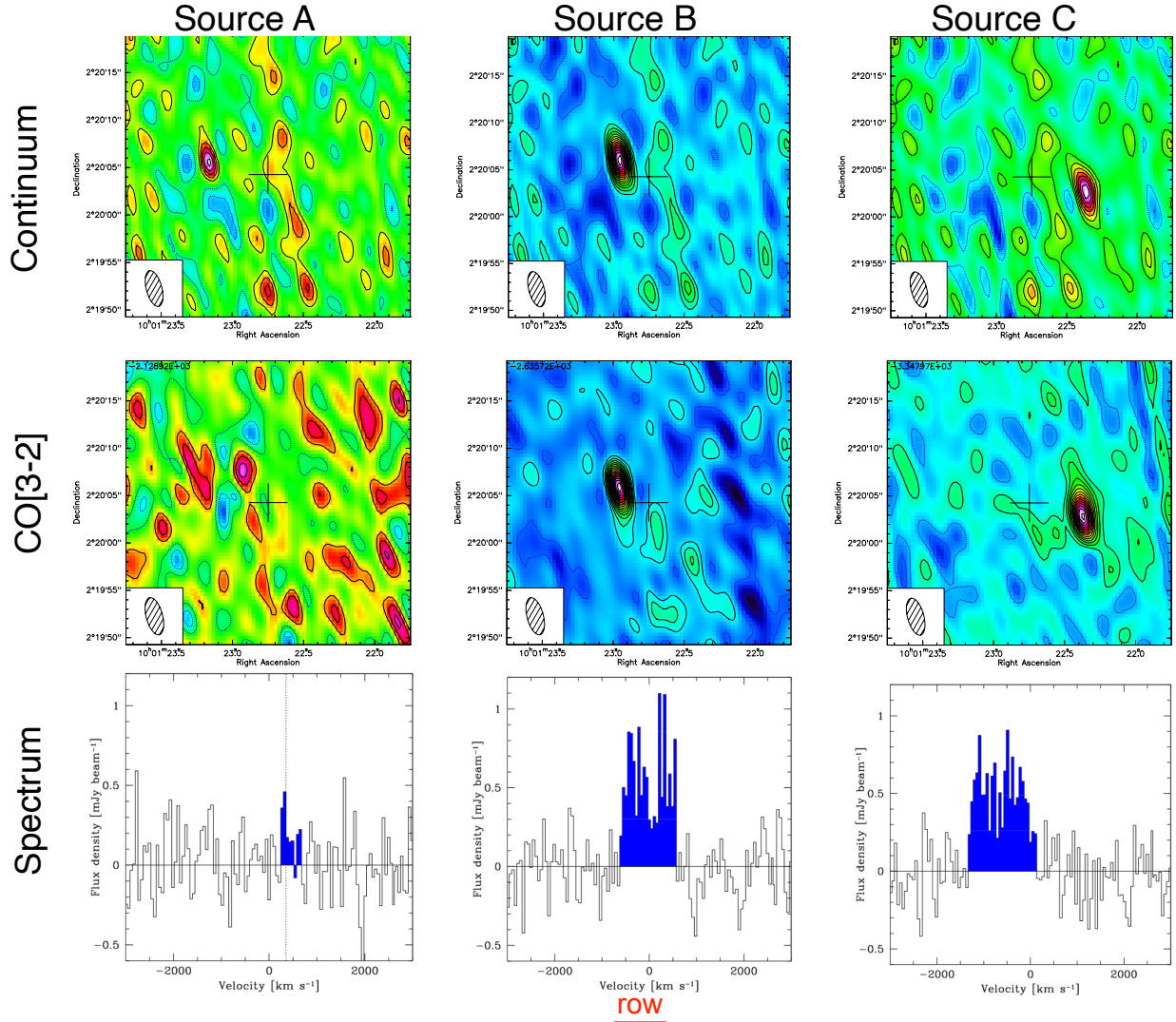


Figure Ex. 2: NOEMA observations. The top line show continuum images, the second are CO[3-2] lines, the third shows the spectra. Different columns correspond to sources A, B, C, as labeled. The spectrum of A, extracted at the well determined continuum position (SN= 8) shows a faint 3.5σ line, at the same velocity of the Ly α at the same position (vertical line). The cross in each map is $\pm 2''$ and shows the position of phase cent

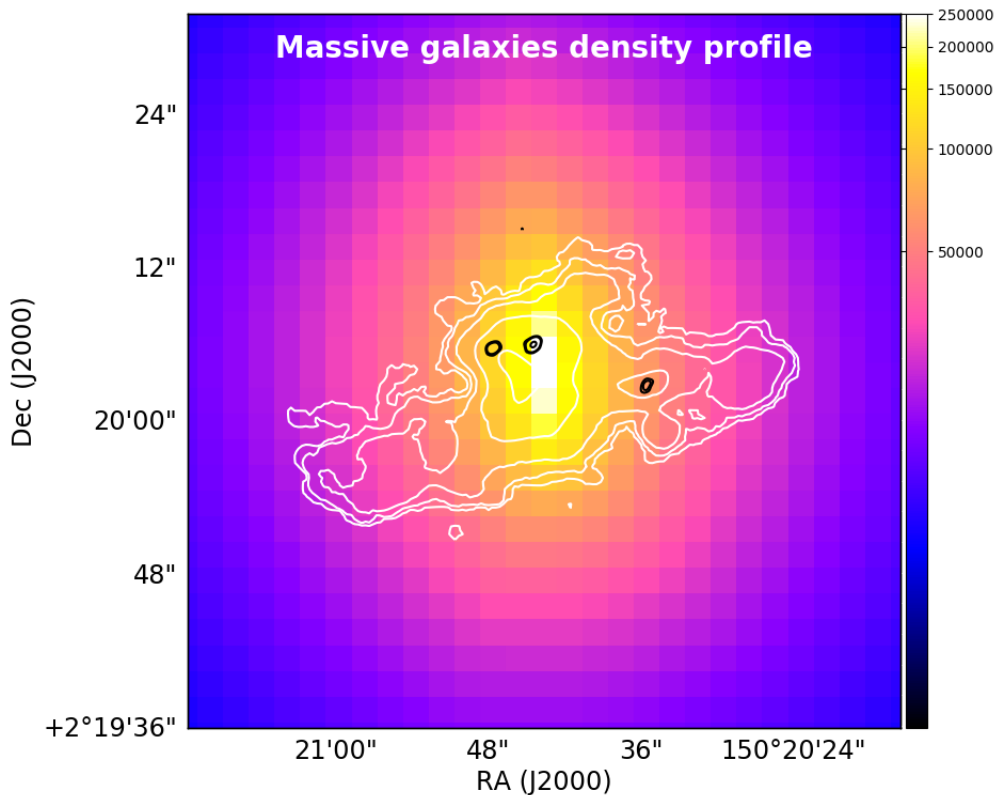


Figure Ex. 3: The 4^{th} -nearest neighbour projected density map of massive galaxies in RO-1001. Notice the excellent coincidence of the Ly α emission (contours) with the potential well of the RO-1001 halo as traced by its massive galaxies. The color scale is in units of number of galaxies per square degree.

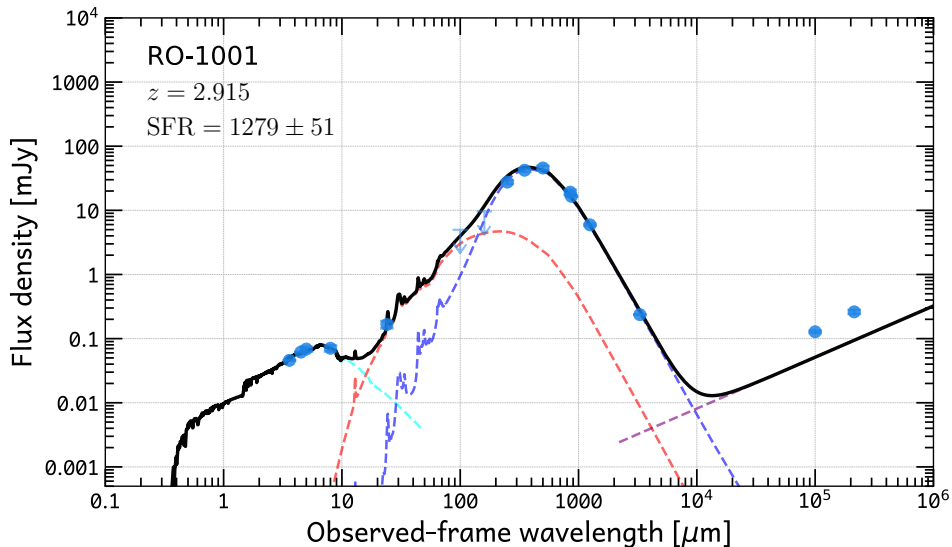


Figure Ex. 4: Integrated spectral energy distribution over the RO-1001 field. The cyan, red and blue curves are BC03 stellar template, DL07 cold (ambient) dust and DL07 warm (PDR) dust, respectively. The radio excess is within a factor of two of the average radio-infrared correlation ([Delhaize](#)) and thus not very significant, but could be associated to galaxy 'C' which shows a somewhat elongated radio morphology suggestive of a weak jet.

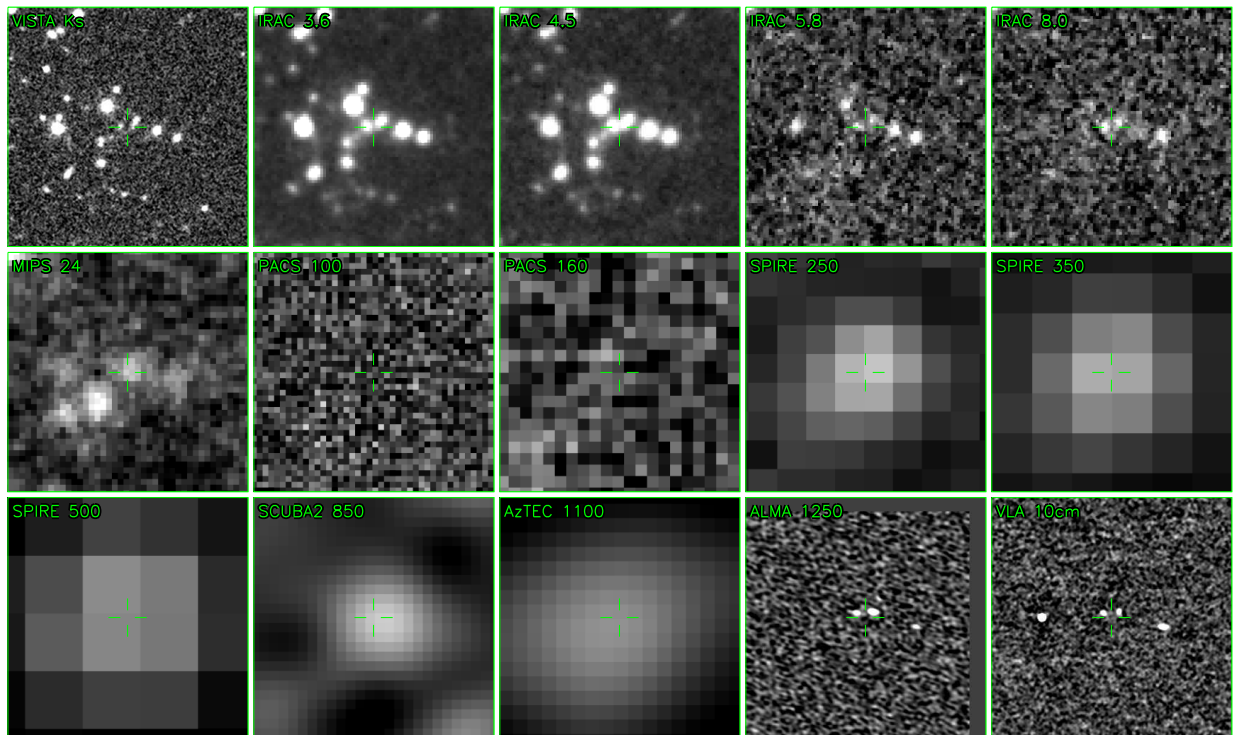


Figure Ex. 5: Multiband imaging of the RO-1001 field from Ks, IRAC, Spitzer, Herschel PACS and SPIRE, SCUBA2, AzTEC, ALMA and radio (as labeled). Each cutout is $50''$ wide.

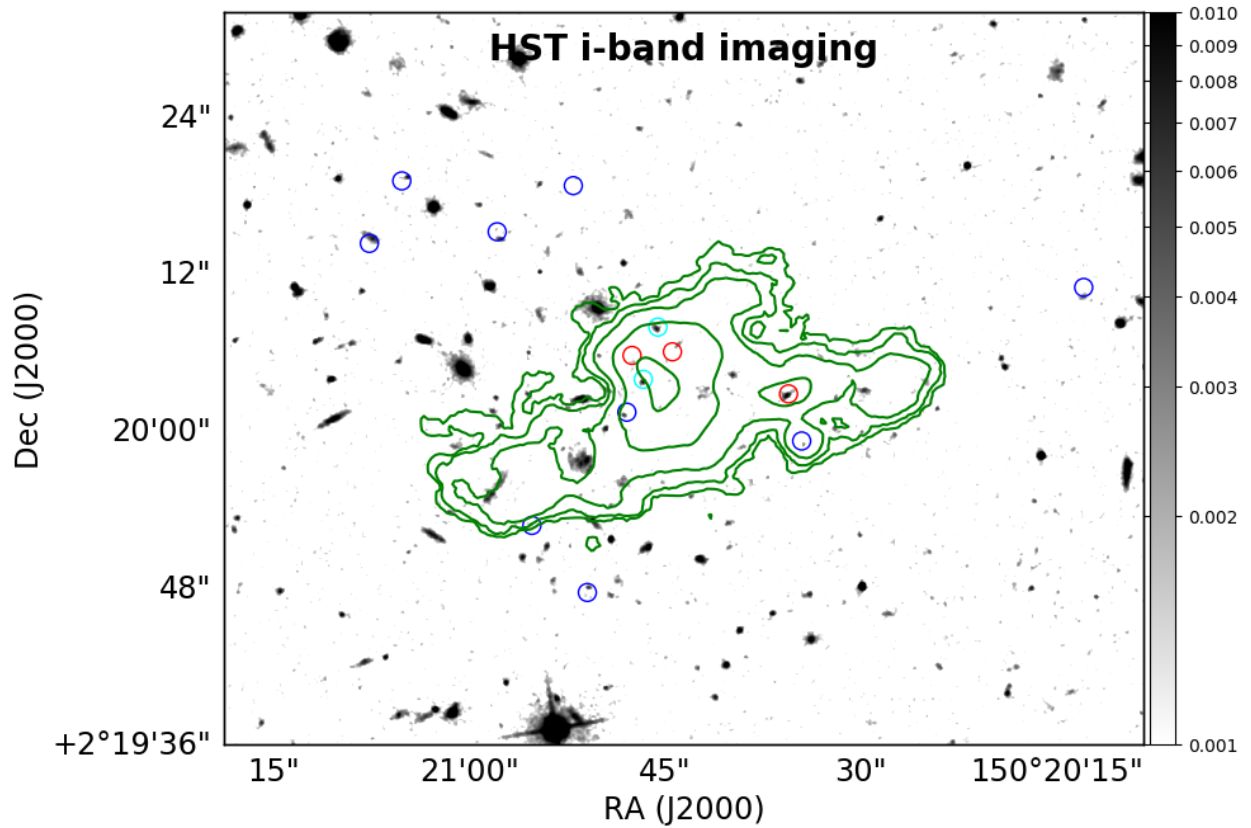


Figure Ex. 6: HST imaging of the field in the F814W filter, single orbit¹⁴. The image is smoothed with the PSF ($0.1''$) to enhance visibility of faint features. Green contours show the Ly α emission. Blue circles are Ly α emitters identified inside the nebula from KCWI data (within 2000 km s^{-1}): the small offsets with respect to the HST positions are a combined effect of the noise in the Ly α cube affecting their recovery and the accuracy of the astrometric solution of the KCWI cube. Cyan circles are two galaxies in the structure identified from UV absorption, red circles show the positions of the ALMA galaxies detections.

Table 1: Massive galaxies in the RO-1001 group

ID	A	B	C	D
RA	10:01:23.174	10:01:22.964	10:01:22.369	10:01:23.438
DEC	02:20:05.57	02:20:05.87	02:20:02.63	02:20:01.10
z_{spec}	2.9214	2.9156	2.9064	2.9 (1)
$\log M^*$	M_{\odot}	11.13	11.13	11.23
SFR (2)	$M_{\odot} \text{ yr}^{-1}$	306	706	266
$S_{\nu}(870\mu\text{m})$	mJy	4.0 ± 0.1	9.1 ± 0.1	3.39 ± 0.15
$S_{\nu}(1.25\text{mm})$	mJy	1.2 ± 0.1	3.4 ± 0.1	1.3 ± 0.2
$S_{\nu}(3.4\text{mm})$	μJy	40 ± 5	88 ± 6	39 ± 5
$S_{\nu}(10\text{cm})$	μJy	38 ± 3	34 ± 3	69 ± 6
$I_{\text{CO}[3-2]}$	$\text{Jy} \times \text{km s}^{-1}$	0.10 ± 0.03	0.69 ± 0.05	0.63 ± 0.05
FWZV $_{\text{CO}[3-2]}$ (4)	km s^{-1}	381	1114	1098
$v_{\text{CO}[3-2]}$ (5)	km s^{-1}	460	13	-690
$r_{1/2}$ (6)	"	0.07 ± 0.01	0.10 ± 0.003	0.11 ± 0.007

Notes: (1) photometric redshifts; (2) derived from the measurement of individual galaxies assuming the same SED shape as for their coaddition (Fig.Ex.4). (3) assuming a linewidth of 500 km s $^{-1}$. (4) Full Width at Zero Velocity corresponding to the full extraction range of the emission line in velocity. (5) systemic velocities of the galaxies are relative to the average, flux weighted redshift of the Ly α emission ($z = 2.9154$). (6) reported sizes are half-light radii from a circular Gaussian fit. Errors are much smaller than the beam size given the high SNR detections. The average size of 0.1" corresponds to 800 pc at $z = 3$.

 Table 2: Gas flows, energetics and Ly α production

Energy source	RO-1001 nebula			QSO nebulae		
	Constrain	Total	Effective	Constrain	Total	Effective
AGN photo.	$L_{\text{AGN}} \lesssim 2 \times 10^{45} \text{ erg s}^{-1}$	$\lesssim 60\%$	$< 20\%$	$L_{\text{AGN}} \sim 10^{47} \text{ erg s}^{-1}$	40	$\approx 1\%$
SF photo.	$1200 M_{\odot} \text{ yr}^{-1}$	5	1%	$120 M_{\odot} \text{ yr}^{-1}$	0.5	< 0.5
AGN outflows	$\lesssim 200 M_{\odot} \text{ yr}^{-1}$	30%	$< 10\%$	$8000 M_{\odot} \text{ yr}^{-1}$	20	$\approx 1\%$
SF outflows	$1200 M_{\odot} \text{ yr}^{-1}$	1	$< 10\%$	$120 M_{\odot} \text{ yr}^{-1}$	negl.	negl.
Gravity	$M_{\text{DM}} = 4 \times 10^{13} M_{\odot}$ $10000 M_{\odot} \text{ yr}^{-1}$	160	$\approx 1\%$	$M_{\text{DM}} = 3 \times 10^{12} M_{\odot}$ $500 M_{\odot} \text{ yr}^{-1}$	≈ 1	$< 1\%$

Total and Effective energy rates for Ly α ionization are given in units of $2 \times 10^{44} \text{ erg s}^{-1}$ for outflows and gravity (the RO-1001 Ly α luminosity and also the typical luminosity of QSO nebulae³) and relative to required numbers of ionizing photons for AGN/SF photoionization. The typical SFR of bright QSO fields is from Reference 62.